Pulse propagation and failure in the discrete FitzHugh-Nagumo model subject to high-frequency stimulation

Irmantas Ratas[1] and Kestutis Pyragas[1,2]
[1]*Center for Physical Sciences and Technology, A. Goštauto 11, LT-01108 Vilnius, Lithuania*
[2]*Department of Theoretical Physics, Faculty of Physics, Vilnius University, LT-10222 Vilnius, Lithuania*
(Received 3 May 2012; published 18 October 2012)

We investigate the effect of a homogeneous high-frequency stimulation (HFS) on a one-dimensional chain of coupled excitable elements governed by the FitzHugh-Nagumo equations. We eliminate the high-frequency term by the method of averaging and show that the averaged dynamics depends on the parameter $A = a/\omega$ equal to the ratio of the amplitude a to the frequency ω of the stimulating signal, so that for large frequencies an appreciable effect from the HFS is attained only at sufficiently large amplitudes. The averaged equations are analyzed by an asymptotic theory based on the different time scales of the recovery and excitable variables. As a result, we obtain the main characteristics of a propagating pulse as functions of the parameter A and derive an analytical criterion for the propagation failure. We show that depending on the parameter A, the HFS can either enhance or suppress pulse propagation and reveal the mechanism underlying these effects. The theoretical results are confirmed by numerical simulations of the original system with and without noise.

DOI: 10.1103/PhysRevE.86.046211 PACS number(s): 05.45.−a, 05.40.Ca, 87.50.−a, 05.90.+m

I. INTRODUCTION

Excitability is observedin a wide range of natural systems, including lasers, chemical reactions, ion channels, cardiovascular tissues, and neural systems. Excitable systems have only one stable fixed point, but perturbations above a certain threshold induce large excursions in phase space, which take the form of spikes of fixed shape. Studding an excitable system under the action of external time-dependent perturbations is an actual problem of physics, neuroscience, physiology and medicine. Various periodic perturbations with periods comparable to the characteristic time scales of an excitable system [1–6], high-frequency (HF) perturbations [7–10], and a combination of low- and high-frequency perturbations [11,12] have been considered in the literature. In this paper we deal with the HF perturbations, which are of particular interest for the problems of neural control. High-frequency alternating currents applied directly to the nerve may produce a reversible conduction block [7,8,13,14]. High-frequency electrical stimulation has been also applied clinically via deep-brain stimulation (DBS) electrodes implanted in specific brain regions to treat movement disorders such as Parkinson's disease and dystonia [15,16]. Although HF DBS has become a well recognized therapeutic procedure, its mechanism of action is still unclear [16–18] and further investigation of how the high-frequency stimulation (HFS) acts on excitable systems is needed.

One of the simplest models of an excitable system that captures many effects observed in neuronal cells is described by the FitzHugh-Nagumo (FHN) equation [19,20]. Recently, we exploited the FHN model to analyze the effect of a homogeneous HFS on nerve pulse propagation in a nonmyelinated axon [10]. We derived analytically the main characteristics of the traveling pulse and showed that with an increase of the amplitude of the HFS current the pulse slows down, shrinks, and disappears when the amplitude exceeds some threshold value. Our analysis was based on the spatially continuous model in which the coupling between the elements of an excitable medium is described by a standard diffusion term. However, most nerve fibers are not a continuous medium but a discrete system of periodic nodes called Ranvier nodes [21]. To model such a myelinated axon the diffusion operator in the FHN equation has to be replaced by the difference operator. The study of the discrete FHN equation is substantially more difficult than that of the continuous version [22–27]. The most significant difference between the discrete and continuous equations is that the discrete system has a coupling threshold for propagation, while the continuous model allows for propagation at all coupling strengths [22].

In this paper we analyze the effect of a homogeneous HFS on pulse propagation in the discrete FHN model. To treat the problem analytically as far as possible we apply the method of averaging [28], which allows us to reduce the original nonautonomous system to autonomous equations. Then we adapt theoretical approaches [21,23,26] developed for the free discrete FHN model. As a result, we obtain the main characteristics of the traveling pulse versus the parameter $A = a/\omega$, which is equal to the ratio of the amplitude a to the frequency ω of the HFS, and derive an analytical criterion for propagation failure. We reveal the significant difference between the results of the action of the HFS on the discrete and continuous FHN models. In the discrete model the HFS can both enhance and suppress pulse propagation, whereas in the continuous model the HFS can cause only suppression.

The rest of the paper is organized as follows. In Sec. II we discuss the model equations and present their reduced (averaged) version. An asymptotic method for constructing pulse solutions of the averaged equations is described in Sec. III. Section IV is devoted to the analysis of pulse characteristics versus the stimulation parameter A. In Sec. V we confirm our theoretical findings by direct numerical simulations of the original system and consider the influence of noise. A summary is presented in Sec. VI.

II. MODEL EQUATIONS

We consider a one-dimensional chain of coupled excitable elements governed by the FitzHugh-Nagumo equations [19, 20] in the presence of a high-frequency field:

$$\dot{v}_n = f(v_n) - w_n + D(v_{n+1} - 2v_n + v_{n-1}) + a\cos(\omega t), \tag{1a}$$

$$\dot{w}_n = \varepsilon(v_n + \beta - \gamma w_n). \tag{1b}$$

These equations represent a paradigmatic model of a spatially discrete excitable medium, which is relevant for different fields of science. To be specific here we discuss Eqs. (1) in the context of a myelinated axon subject to the HFS. Then the variable v_n denotes the membrane potential and w_n is the recovery variable of the nth node of Ranvier, $f(v_n) = v_n - v_n^3/3$ is the cubic source term of an ionic current, and the discrete diffusive term with the coupling strength D is proportional to the difference in internodal currents through a given site. The last term in Eq. (1a) describes the current induced by HFS, where a and ω are the amplitude and the frequency, respectively. The constant $\varepsilon > 0$ is the ratio between the characteristic time scales of v_n and w_n variables. As usual, we assume $\varepsilon \ll 1$, that is, fast excitation and slow recovery. We select the parameters γ and β such that without a HFS current the neuron is in an excitable regime. In this paper numerical simulations are performed for $\gamma = 0.8$ and $\beta = 0.7$.

The analysis of the system (1) can be greatly simplified if we assume that the period $T = 2\pi/\omega$ of the HFS is much less than the characteristic time scales of the FHN axon. In this case, the high-frequency term in Eq. (1a) can be eliminated via a two-scale expansion method [29] in a way similar to what has been done in our recent paper [10] for the continuous version of FHN equations. In the Appendix, however, we present an alternative approach based on the method of averaging [28]. Both methods lead to the same result, but the latter is most straightforward and allows us to define the criteria of validity of the averaged equations in a more rigorous way.

According to the results presented in the Appendix, an approximate solution of Eqs. (1) can be written as a sum of slow (averaged over the stimulation period) and fast (harmonic) components

$$v_n(t) \approx \bar{v}_n(t) + A\sin(\omega t), \tag{2a}$$

$$w_n(t) \approx \bar{w}_n(t). \tag{2b}$$

The variables $\bar{v}_n$ and $\bar{w}_n$ satisfy the averaged equations

$$\dot{\bar{v}}_n = \bar{f}(\bar{v}_n) - \bar{w}_n + D(\bar{v}_{n+1} - 2\bar{v}_n + \bar{v}_{n-1}), \tag{3a}$$

$$\dot{\bar{w}}_n = \varepsilon(\bar{v}_n + \beta - \gamma\bar{w}_n), \tag{3b}$$

which are similar to Eqs. (1), but they do not contain the HFS current. The elimination of the HFS current, however, changes the ionic current function $f(v)$, which now takes the form $\bar{f}(\bar{v}_n) = (1 - A^2/2)\bar{v}_n - \bar{v}_n^3/3$. The parameter A, which is equal to the ratio of the amplitude to the frequency of the stimulating current

$$A = a/\omega, \tag{4}$$

completely defines the effect of the HFS on the averaged neuron dynamics. When the HFS is switched off ($a = 0$ or $A = 0$), Eqs. (3) coincide with the original equations (1); however, when the HFS is on, the term $-\bar{v}_n A^2/2$ in the nonlinear function $\bar{f}(\bar{v}_n)$ modifies the nullcline of Eq. (3a) and changes the excitability properties of the neuron (see Ref. [10] for details). We emphasize that the approximate solution (2) is valid only for large frequencies $\omega \gg 1$ since terms of accuracy of $O(\omega^{-1})$ are neglected. A comparison of solutions of the original equations (1) and the averaged system (3) is demonstrated in Fig. 1(a).

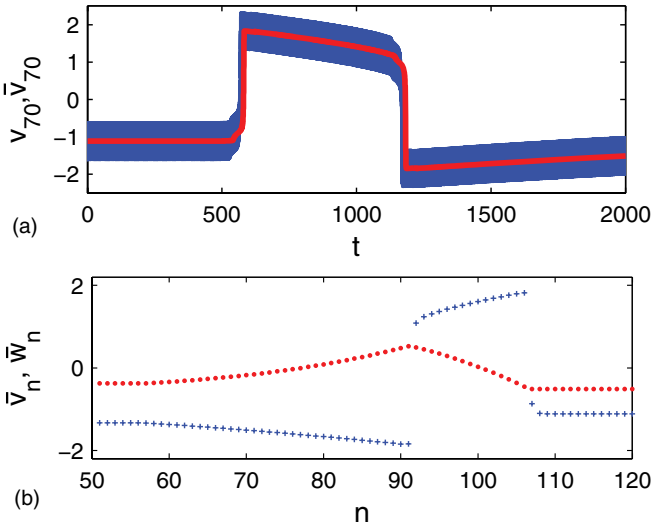

FIG. 1. (Color online) (a) Comparison of the solutions of the original equations (1) and the averaged equations (3). The dynamics of the membrane potential for the 70th node of the axon obtained from the original and averaged systems are shown by dark gray (blue) (the HF oscillations are not resolved) and light gray (red) curves, respectively. (b) Snapshot of a typical pulse propagating from left to right computed from the averaged system (3). The membrane potential and recovery variables are marked by the dots (red) and crosses (blue), respectively. The parameters are $a = 5$, $\omega = 10$, $A = 0.5$, $D = 0.015$, and $\varepsilon = 0.0008$.

III. ASYMPTOTIC CONSTRUCTION OF PULSE SOLUTIONS

The method of averaging has allowed us to reduce the original problem to the analysis of the averaged equations (3). These equations are autonomous, and we can utilize theoretical approaches developed for the free discrete FHN system. In the following we are interested in estimating characteristic parameters of the propagating pulses versus the stimulation parameter A and finding a criterion for propagation failure. Note that if the averaged equations (3) have a solution with a propagating pulse, then in the original system this pulse will propagate against the background of homogeneous high-frequency oscillations described by the term $A\sin(\omega t)$ in Eq. (2a).

An asymptotic construction of pulse solutions for the free discrete FHN equation in the limit $\varepsilon \to 0$ is described in Ref. [26]. The main idea is similar to Keener's asymptotic idea [30] developed for the FHN model with spatially continuous diffusion. We combine these ideas with the Erneux-Nicolis [23] perturbation theory developed for the discrete Nagumo model to study pulse propagation in the averaged system (3).

A snapshot of a typical propagating pulse computed from the system (3) is shown in Fig. 1(b). The pulse profile can be subdivided into four segments. There are two segments in which $\bar{v}_n$ vary smoothly with n, separated by two moving sharp fronts usually called the leading and trailing edges. We refer to the segment between the fronts as the pulse overshoot and to the segment following the trailing edge as the pulse undershoot. In the latter two segments we may set $\dot{v}_n = 0$ and $D = 0$ and obtain a description of slow recovery. Wave fronts are smooth solutions $\bar{v}_n(t) = \bar{v}(z)$ and $\bar{w}_n(t) = \bar{w}(z)$ of the continuous variable $z = n - ct$, where c is the pulse speed. The recovery variable $\bar{w}$ is constant at each side of the front and the excitation variable is governed by the discrete Nagumo equation (3a). A stable pulse is obtained when the velocity of the leading edge is equal to the velocity of the trailing edge.

For further analysis we rewrite Eqs. (3) in a more convenient form. For $D = 0$ these equations have the only fixed point $(\bar{v}_n, \bar{w}_n) = (V_0, W_0)$, where $W_0 = (V_0 + \beta)/\gamma$ and V_0 is the resting potential of the neuron that satisfies the real-value solution of the cubic equation

$$V_0^3/3 - V_0(1 - 1/\gamma - A^2/2) + \beta/\gamma = 0. \tag{5}$$

We define the deviations from the fixed point as $(\delta v_n, \delta w_n) = (\bar{v}_n - V_0, \bar{w}_n - W_0)$ and rewrite Eqs. (3) for these deviations

$$\delta\dot{v}_n = F(\delta v_n) - \delta w_n + D(\delta v_{n+1} - 2\delta v_n + \delta v_{n-1}), \tag{6a}$$

$$\delta\dot{w}_n = \varepsilon(\delta v_n - \gamma\delta w_n), \tag{6b}$$

where $F(\delta v_n) = \delta v_n(1 - A^2/2 - V_0^2) - \delta v_n^2 V_0 - \delta v_n^3/3$ is a cubic polynomial function. This polynomial has three real-value roots, one of which is equal to zero. Therefore, the polynomial $F(\delta v_n)$ can be factorized as

$$F(\delta v_n) = -\delta v_n(\delta v_n - V_1)(\delta v_n - V_2)/3, \tag{7}$$

where the two other roots V_1 and V_2 of the polynomial are positive and can be simply determined from a quadratic equation

$$V_{1,2} = \tfrac{1}{2}\big(-3V_0 \pm \sqrt{12 - 6A^2 - 3V_0^2}\big). \tag{8}$$

Note that the middle root V_2 of the polynomial (7) has a clear physical meaning. It defines an excitability threshold of the neuron. Indeed, an uncoupled excitable element described by the system (6) for $D = 0$ has the only stable fixed point $(\delta v_n, \delta w_n) = (0,0)$. If we excite the membrane potential by an amount δv_n^0, i.e., take the initial conditions $(\delta v_n^0, 0)$, then the excitable element will generate the spike only if δv_n^0 exceeds the threshold value V_2. In the following we refer to V_2 as an excitability threshold. We will see that due to the dependence of V_2 on the stimulation parameter A, the HFS allows for the efficient control of pulse propagation in the coupled excitable elements.

We can now discuss different segments in the asymptotic description ($\varepsilon \to 0$) of a pulse as follows (see Ref. [26]).

(i) *The leading edge*. Here the membrane potential δv_n varies rapidly, while the recovery variable is fixed at $\delta w_n = 0$, so Eqs. (6) reduce to

$$\delta\dot{v}_n = F(\delta v_n) + D(\delta v_{n+1} - 2\delta v_n + \delta v_{n-1}). \tag{9}$$

This equation admits a solution in the form of a wave front moving towards the right $\delta v_n(t) = \delta v(n - ct)$ with speed c measured in nodes per unit time t. The monotonically decreasing profile $\delta v(z)$ satisfies the boundary conditions $\delta v(-\infty) = V_1$ and $\delta v(\infty) = 0$. Below we will use Eq. (9) to derive the criterion for propagation failure and to estimate the pulse speed for small and large coupling strength D.

(ii) *The pulse overshoot*. This is a segment between the fronts in which the variation of the fast variable δv_n can be neglected. Taking $D(\delta v_{n+1} - 2\delta v_n + \delta v_{n-1}) = 0$ and $\delta\dot{v}_n = 0$ in Eq. (6a), we obtain the relationship between δv_n and δw_n

$$\delta w_n = F(\delta v_n). \tag{10}$$

The inverse relationship $\delta v_n = R(\delta w_n)$ can be obtained by solving the cubic equation (10) with respect to δv_n. We numerate the roots of this equation in increasing order as $R_1(\delta w_n) < R_2(\delta w_n) < R_3(\delta w_n)$. The slow recovery variable obeys Eq. (6b) with $\delta v_n = R_3(\delta w_n)$:

$$\delta\dot{w}_n = \varepsilon[R_3(\delta w_n) - \gamma\delta w_n], \tag{11}$$

where $R_3(\delta w_n)$ is the largest root of Eq. (10). This segment contains a finite number of nodes. On its far right $\delta w_n = 0$. As we move towards the left, δw_n increases slowly until it reaches a certain value $\delta\tilde{w}$ corresponding to that in the trailing wave front. The value $\delta\tilde{w}$ is determined from the condition that the leading and trailing edges move with the same speed. Equations (10) and (11) will be used below to estimate the length of the pulse overshoot.

(iii) *The trailing edge*. Here the recovery variable is fixed at $\delta w_n = \delta\tilde{w}$, while the dynamics of the variable δv_n is governed by

$$\delta\dot{v}_n = \tilde{F}(\delta v_n) + D(\delta v_{n+1} - 2\delta v_n + \delta v_{n-1}), \tag{12}$$

where

$$\tilde{F}(\delta v_n) = F(\delta v_n) - \delta\tilde{w} \tag{13}$$

is a cubic polynomial with respect to δv_n whose roots we denote by $\tilde{R}_1 < \tilde{R}_2 < \tilde{R}_3$. We are interested in solution of Eq. (12) in the form of a moving trailing front $\delta v_n(t) = \delta v(n - ct)$ with the boundary conditions $\delta v(-\infty) = \tilde{R}_1$ and $\delta v(\infty) = \tilde{R}_3$. Now the speed c of the front depends on the parameter $\delta\tilde{w}$. To obtain the appropriate value of this parameter the dependence $c = c(\delta\tilde{w})$ has to be numerically estimated from Eq. (12). Then the correct value $\delta\tilde{w}$ is determined from the requirement $c(\delta\tilde{w}) = c(0)$, which means that the leading and trailing edges move with the same speed. As mentioned above, the value $\delta\tilde{w}$ is needed to estimate the pulse length.

(iv) *The pulse undershoot*. This segment corresponds to the pulse tail. Here the recovery variable obeys Eq. (6b) with $\delta v_n = R_1(\delta w_n)$:

$$\delta\dot{w}_n = \varepsilon[R_1(\delta w_n) - \gamma\delta w_n], \tag{14}$$

where $R_1(\delta w_n)$ is the least root of Eq. (10). Equation (14) describes a slow relaxation of δw_n from the initial state $\delta w_n = \delta\tilde{w}$ to the state $\delta w_n = 0$. We will use this equation to estimate the length of the pulse undershoot.

The above approximations constitute the basis for our further analysis.

IV. PULSE CHARACTERISTICS AND PROPAGATION FAILURE AS FUNCTIONS OF THE STIMULATION PARAMETER A

We are seeking to define the main characteristics of the pulse as functions of the stimulation parameter A. We are also interested in the criterion of propagation failure. There are two factors responsible for this phenomenon. The first is inherent in discrete systems and may come into play if the coupling strength D is too small and/or the excitability threshold V_2 is too large. For $\varepsilon = 0$ this factor can be analyzed based on the Nagumo equation (9). There exists a critical value $D = D_c$ below which the leading front fails to propagate [22,23]. In Sec. IV A we will establish the dependence of the critical coupling D_c on the stimulation parameter A.

The second factor responsible for propagation failure is related to the finite value of ε, when the recovery is not sufficiently slow. This phenomenon also occurs in the spatially continuous FHN system. The continuous system possesses two pulses (one stable and the other unstable), which coalesce at a certain critical value of $\varepsilon = \varepsilon_c$ and cease to exist for $\varepsilon > \varepsilon_c$ [10]. In the discrete FHN system, the propagation failure occurs due to the finite number of nodes inside the pulse [26]. With an increase of ε, the length of the pulse decreases and the pulse ceases to exist when its length becomes less than the distance between the nodes. We will discuss this type of propagation failure in Sec. IV C.

A. Propagation failure for $\varepsilon = 0$

First, we establish a criterion when the leading front (consequently, also the pulse) cannot propagate in the system. For $\varepsilon = 0$ the leading front is governed by the discrete Nagumo equation (9). This equation has been extensively studied in the literature and various algorithms for finding approximate solutions have been introduced. Here we extend the ideas of the perturbation theory proposed in Ref. [23] and derive a criterion for propagation failure versus the stimulation parameter A. To simplify the analysis, we reduce the number of parameters in Eq. (9) by the following substitutions: $V_2/V_1 = q$, $3D/V_1^2 = d$, $V_1 t/3 = \tau$, and $\delta v_n/V_1 = u_n$. Then Eq. (9) transforms to

$$du_n/d\tau = \psi(u_n) + d(u_{n+1} - 2u_n + u_{n-1}), \tag{15}$$

where

$$\psi(u_n) = -u_n(u_n - 1)(u_n - q). \tag{16}$$

Equations (15) and (16) contain only two parameters q and d. To use the ideas of perturbation theory [23], we assume that q is a small parameter compared to 1. This assumption is satisfactory if the stimulation parameter A is not very large. In this section we are mainly interested in values of $A \in (0,1.2)$; then q varies in the interval $(0.12,0.23)$.

To determine the conditions for a traveling front solution, we consider a set of $N+2$ elements described by Eq. (15) for $n = 1,\ldots,N$ and the boundary conditions for the first and last nodes as

$$u_0 = 1, \quad u_{N+1} = u_N. \tag{17}$$

The front solution joining two stable points $u_n = 1$ and 0 can be originated by the initial condition: $u_n = 0$ for $n = 1,\ldots,N$ at $t = 0$. If there is no coupling between the nodes ($d = 0$), the initial front remains pinned for all times $t > 0$. However, if we increase d to some critical value $d = d_c(q)$, the front starts to propagate. The critical value d_c can be estimated by the bifurcation analysis of the steady-state solutions of Eq. (15).

The idea of the bifurcation analysis can be demonstrated with the simple example of a neuron consisting of only three elements. In this case $N = 1$ and we have the only dynamic equation for u_1: $du_1/d\tau = \psi(u_1) + d(1 - u_1)$. For $d = 0$ this system has two stable fixed points $u_1 = 0$ and 1 and one unstable fixed point $u_1 = q$. With the increase of d, the points $u_1 = 0$ and q approach each other and coalesce at the saddle-node bifurcation for some $d = d_c$, so for $d > d_c$ the only stable fixed point $u_1 = 1$ remains in the system. The critical value d_c can be determined from the equations $\Psi_1 \equiv \psi(u_1) + d(1 - u_1) = 0$ and $d\Psi_1/du_1 = 0$. Solving these equations we obtain $d_c = q^2/4$. This expression has been derived in Ref. [23]; it is valid for a neuron with an arbitrary number of nodes with accuracy of $O(q^2)$. In the following we refine this expression by expanding it with higher-order terms with respect to q.

To derive higher-order terms in the expression $d_c = d_c(q)$ we have to generalize the above consideration for a neuron consisting of an arbitrary number of nodes. When the number of nodes in a neuron is $N+2$ the saddle-node bifurcation initiating the front propagation takes place in an N-dimensional phase space defined by the state vector $\mathbf{X} = (x_1, x_2, \ldots, x_N)$. The fixed points, having coordinates $(0,0,\ldots,0)$ and $(q,0,\ldots,0)$ at $d = 0$, coalesce at $d = d_c$ when the right-hand side (rhs) of Eq. (15) and its Jacobian vanish:

$$\psi(u_n) + d(u_{n+1} - 2u_n + u_{n-1}) = 0, \quad n = 1,\ldots,N, \tag{18}$$

$$\begin{vmatrix} \psi'(u_1) - 2d & d & 0 & \cdots & 0 & 0 \\ d & \psi'(u_2) - 2d & d & \cdots & 0 & 0 \\ \vdots & \vdots & \vdots & \ddots & \vdots & \vdots \\ 0 & 0 & 0 & \cdots & d & \psi'(u_N) - d \end{vmatrix} = 0. \tag{19}$$

Equations (18) and (19) together with the boundary conditions (17) define completely the conditions of the saddle-node bifurcation for arbitrary N.

For small q these equations can be solved by expanding $d = d_c(q)$ and $u_n(q)$ in power series of the parameter q. The analysis of low-dimensional cases $N = 1,2$ suggests that $d_c = O(q^2)$ and $u_n = O(q^n)$. This motivates the following general expansions:

$$d_c = \sum_{k=0}^{\infty} q^{2+k} d^{(k)}, \quad u_n = \sum_{k=0}^{\infty} q^{n+k} u_n^{(k)}. \tag{20}$$

Substituting Eqs. (20) into Eqs. (18) and (19) and equating terms at different powers of q, one obtains the expansion coefficients $d^{(k)}$ and $u_n^{(k)}$ in an explicit form. Performing this procedure up to third-order terms in the expansion of d_c, we get

$d^{(0)} = 1/4$, $d^{(1)} = 1/8$, $d^{(2)} = 7/64$, $u_1^{(0)} = 1/2$, $u_1^{(1)} = 1/8$, $u_1^{(2)} = 5/32$, and $u_2^{(0)} = 1/8$. As a result we obtain the critical value of the coupling strength up to terms proportional to q^4:

$$d_c = \frac{q^2}{4}\left(1 + \frac{1}{2}q + \frac{7}{16}q^2\right) \tag{21}$$

or in original variables

$$D_c = \frac{V_2^2}{12}\left[1 + \frac{1}{2}\frac{V_2}{V_1} + \frac{7}{16}\left(\frac{V_2}{V_1}\right)^2\right]. \tag{22}$$

Equation (22) together with Eqs. (5) and (8) gives an analytical dependence of the critical coupling strength D_c on the stimulation parameter A. This dependence is depicted in Fig. 2. The dashed curve shows this dependence estimated from the first-order term $V_2^2/12$ in Eq. (22), while the solid curve takes into account all three terms in expansion (22). The critical values of the coupling strength obtained directly by numerical simulation of the Nagumo equation (9) are shown by symbols. We see that the analytical formula (22) agrees well with the numerical experiments.

An important property of the dependence $D_c = D_c(A)$ is the presence of a dip in a certain interval of A: With an increase of A the D_c first falls to a minimal value $D_c^* = D_c(A^*)$ at $A = A^*$ and then increases for $A > A^*$. Such a dependence allows us to enhance the conductivity of a neuron by choosing an appropriate value of the parameter A. Indeed, if we take the value D of the coupling strength from the interval $[D_c^*, D_c(0)]$, then the pulse cannot propagate without HFS since $D < D_c(0)$. However, if we increase A so that its value ends up in the interval $A_1 < A < A_2$, where $D_c(A_1) = D_c(A_2) = D$, then the propagation becomes possible. For $A > A_2$ the propagation will be suppressed again.

We emphasize that the effect of enhancement of pulse propagation by HFS is an exclusive property of spatially discrete systems. This is because the difference operator that

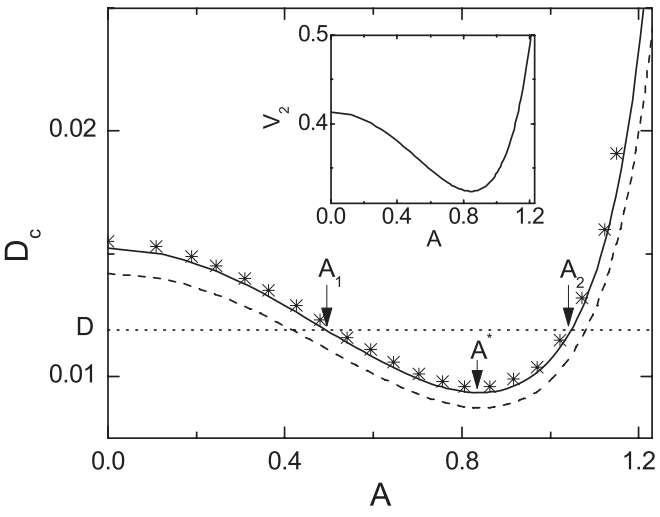

FIG. 2. Critical coupling strength D_c as a function of the stimulation parameter A. The dashed curve represents an approximation with only the first term in expansion (22), the solid curve takes into account all three terms in expansion (22), and asterisks show the results of direct numerical simulation of Eq. (9). The inset shows the dependence of the excitability threshold V_2 on A.

describes the coupling between the nodes can be approximated by the diffusion operator only in the limit $D \to \infty$, whereas this effect takes place only for small D, when $D < D_c(0)$. For $D > D_c(0)$, the HFS may cause only suppression.

The mechanism of enhancement of pulse propagation can be explained as follows. If we omit higher-order terms in expansion (22), then we reveal that the critical coupling strength D_c is proportional to the square of the neuron excitability threshold $D_c \propto V_2^2$. Therefore, the dip in the dependence of D_c on A is caused by a similar dependence of the excitability threshold V_2 on A. The dependence $V_2 = V_2(A)$ is shown in the inset of Fig. 2. We see that in a certain interval of the stimulation parameter A, the HFS reduces the excitability threshold of excitable elements and this enhances the pulse propagation. Similarly, the suppression of pulse propagation for large A is explained by the sudden increase of the excitability threshold $V_2(A)$ for $A > A^*$.

B. Pulse speed

The speed of the pulse is determined by the discrete Nagumo equation (9) that describes the motion of the leading front. Analytical expressions for the front speed of the discrete Nagumo equation have been derived for two cases: (i) for small coupling strength, when D is close to the critical value D_c [23], and (ii) for large D, when the difference operator in the Nagumo equation can be approximated by the diffusion operator and a small correction term [21]. Here we utilize these theoretical results to estimate the dependence of the front speed on the stimulation parameter A.

For d close to d_c the front speed of the Nagumo system written in the form of Eq. (15) has been derived in Ref. [23]. In the notations of Eq. (9) this reads

$$c = \frac{\sqrt{3(D - D_c)}}{V_1\{\arctan[V_2\sqrt{3/(D - D_c)}/6] + \pi/2\}}. \tag{23}$$

For large D the expression for the front speed can be found in Ref. [21]:

$$c = c_0\sqrt{D}\left[1 - \tau_1(c_0)c_0^2/2D\right], \tag{24}$$

where

$$c_0 = (V_1 - 2V_2)/\sqrt{6} \tag{25}$$

and $c_0\sqrt{D}$ is the front speed in the spatially continuous case. The coefficient $\tau_1(c_0)$ depends on the front profile and can be computed according to the algorithm described in Ref. [21] (p. 279).

In Fig. 3 we show the dependence of the front speed on the stimulation parameter A computed from Eqs. (23) and (24) for small and large values of the coupling strength, respectively. We compare these analytical results with the results of direct numerical simulation of Eq. (9). We see that the accuracy of Eq. (23) is good in the regions of the parameter A, where the front speed approaches zero, i.e., close to the thresholds of the propagation failure, and the accuracy declines beyond these regions. For large D the discrete system can be well approximated by the continuous model and Eq. (24) provides an accurate estimate of the front speed for all A.

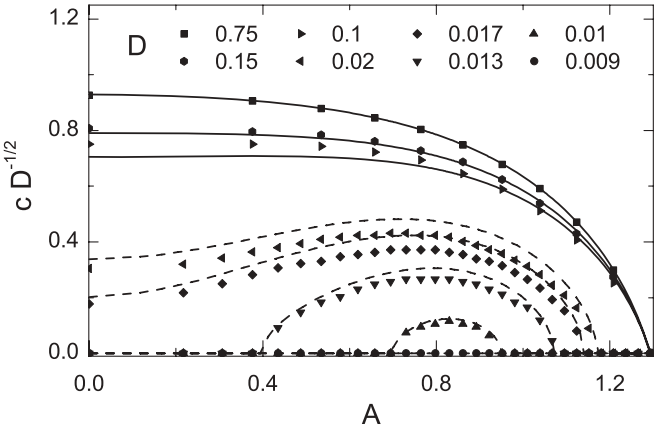

FIG. 3. Scaled front speed $cD^{-1/2}$ as a function of the stimulation parameter A for different values of the coupling strength D. The dashed and solid curves represent analytical results obtained from Eqs. (23) and (24), respectively. The symbols show the results of numerical simulation of Eq. (9).

C. Pulse length and propagation failure for a finite ε

For the spatially discrete system, the durations of the pulse overshoot T_O and undershoot T_U can be estimated in a manner similar to that in the spatially continuous case (see Refs. [21, 26]):

$$T_O = \int_0^{\delta\tilde{w}} \frac{d\delta w_n}{\varepsilon[R_3(\delta w_n) - \gamma\delta w_n]}, \tag{26}$$

$$T_U = \int_{\delta\tilde{w}}^{0} \frac{d\delta w_n}{\varepsilon[R_1(\delta w_n) - \gamma\delta w_n]}. \tag{27}$$

Equations (26) and (27) follow from Eqs. (11) and (14), respectively. The lengths of the pulse overshoot L_O and undershoot L_U measured in a number of nodes per corresponding segment can be estimated by multiplying the above times with the pulse speed:

$$L_O = cT_O = \frac{c}{\varepsilon}\int_{V_1}^{\tilde{R}_3} \frac{F'(\delta v_n)d\delta v_n}{\delta v_n - \gamma F(\delta v_n)}, \tag{28}$$

$$L_U = cT_U = \frac{c}{\varepsilon}\int_{\tilde{R}_1}^{0} \frac{F'(\delta v_n)d\delta v_n}{\delta v_n - \gamma F(\delta v_n)}. \tag{29}$$

Here the integral expressions are rewritten in a form convenient for numerical estimation. The integration variable δw_n is replaced by δv_n taking into account the relationship (10). The $F'(\delta v_n)$ denotes the derivative of the function $F(\delta v_n)$. Note that the lengths L_O and L_U decrease as ε^{-1} with the increase of ε and the pulse ceases to exist at some $\varepsilon = \varepsilon_c$ when the shorter length L_O falls below 1. This condition defines a simple criterion for the pulse propagation failure at finite ε.

In Figs. 4(a) and 4(b) we show the dependence of εL_O on the stimulation parameter A for different D. The solid curves are obtained from Eq. (28), while the symbols denote the results of direct numerical simulation of the averaged system (3). In fact, the variable εL_O provides an estimate for the critical value of the parameter ε at which the pulse ceases to exist, since $\varepsilon L_O = \varepsilon_c$ when $L_O = 1$. For large D [Fig. 4(a)] the dependence of ε_c on A is monotonic and thus the HFS

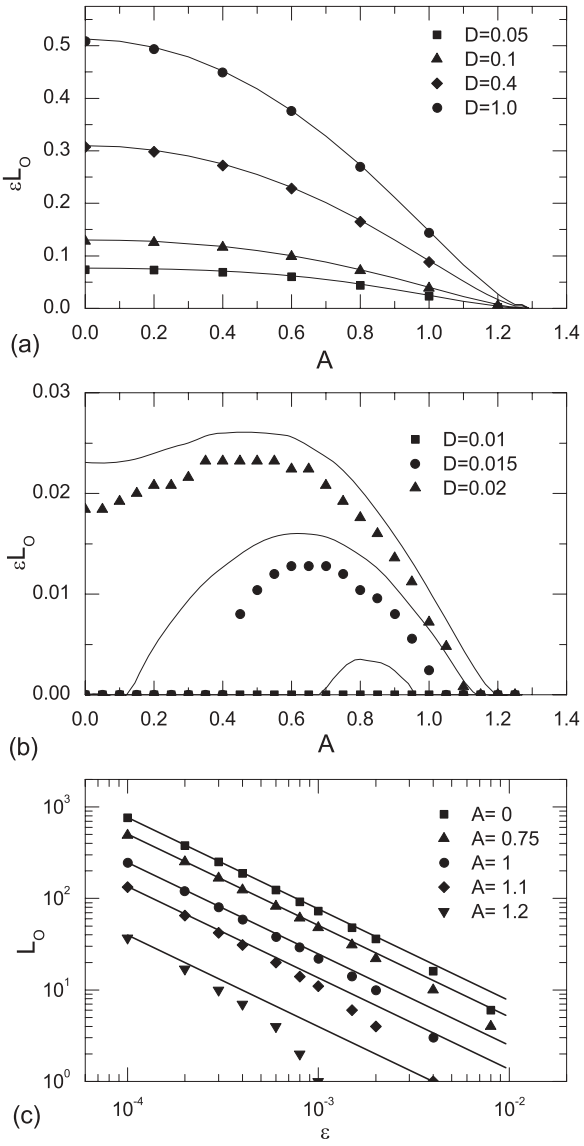

FIG. 4. (a) and (b) Length of the pulse overshoot multiplied by ε as a function of the stimulation parameter A for different values of the coupling strength D. (c) Dependence of the length of the pulse overshoot on ε for fixed $D = 0.05$ and different values of A. Solid curves represent estimations based on formula (28), while symbols show the results of direct numerical simulations of the averaged system (3). The length of the pulse in (a) and (b) has been estimated from Eq. (3) for $\varepsilon = 0.0008$.

can cause only suppression of pulse propagation. For small D [Fig. 4(b)] the nonmonotonic dependence of ε_c on A makes possible both effects: the enhancement and suppression of the propagation. Note that for large D Eq. (28) approximates well the results of the averaged system (3), while for small D the accuracy of Eq. (28) declines.

To verify the law of proportionality $L_O \propto \varepsilon^{-1}$ anticipated by Eq. (28), in Fig. 4(c) we present the dependence L_O on ε (for different values of A) on a double logarithmic scale. Then this dependence should take the form of straight lines. As seen from the figure, the direct numerical simulations of the averaged equations (3) indeed support this law for sufficiently small values of ε.

V. NUMERICAL SIMULATIONS OF THE ORIGINAL SYSTEM

In the preceding section we have shown that the asymptotic theory described in Sec. III predicts rather well the properties of the averaged system (3) provided the parameter ε is sufficiently small. We recall that the system (3) has been derived from the original equations (1) using the method of averaging. To support the validity of this approximation, we now confirm the main effects of the HFS observed in the averaged system (3) by numerical simulations of the original system (1).

In Fig. 5 we show the solutions of Eqs. (1), which demonstrate the effect of enhanced pulse propagation under the action of HFS. The value of the coupling strength is chosen sufficiently small $D = 0.015$ so that for $\varepsilon = 0.0008$ the pulse cannot propagate in the free ($A = 0$) system. The simulations were performed with the boundary conditions $v_0 = v_1$ and $v_{N+1} = v_N$. The initial conditions for all elements were chosen to be equal to the fixed point of the averaged equations at the given stimulation intensity except for ten nodes in the middle of the sample, where the potential variable was enlarged by 2. In Fig. 5(a) the stimulation is off ($A = 0$) and the initial excitation of the middle nodes dies out, while in Fig. 5(b) the HFS with the stimulation parameter $A = 0.7$ cancels the propagation failure and we observe two pulses propagating in different directions.

In order to test the influence of noise on the above effect, we performed simulations of the system (1) with a modified Eq. (1b):

$$\dot{w}_n = \varepsilon[v_n + \beta - \gamma w_n + \sigma\xi_n(t)]. \tag{30}$$

We added the white Gaussian noise term $\sigma\xi_n(t)$ with $\langle\xi_n(t)\rangle = 0$ and $\langle\xi_n(t)\xi_{n'}(t')\rangle = \delta_{n,n'}\delta(t-t')$. Here the parameter σ governs the amplitude of noise, $\delta_{n,n'}$ is the Kronecker delta function, and $\delta(t)$ is the Dirac delta function. The results of simulations are presented in Figs. 5(c) and 5(d). The small noise intensity $\sigma = 0.1$ in Fig. 5(c) does not influence the effect. However, sufficiently large noise may destroy the pulse propagation. In Fig. 5(d) we see that for $\sigma = 0.5$ the pulse propagating to the right dies out, while the pulse propagating to the left is not destroyed.

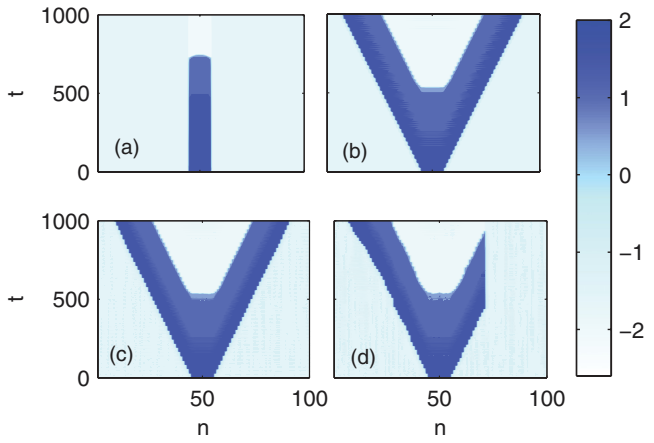

FIG. 5. (Color online) Spatiotemporal evolution of the membrane potential (a) and (b) without noise [Eqs.(1)] and (c) and (d) in the presence of noise [Eqs. (1a) and (30)]. The background of homogeneous high-frequency oscillations is excluded by subtracting from the membrane potential the term $A\sin(\omega t)$ [see Eq. (2a)], i.e., the color encodes the value $v_n - A\sin(\omega t)$. The values of the fixed parameters are $\omega = 10$, $N = 100$, $\varepsilon = 0.0008$, and $D = 0.015$. The variable parameters are (a) $A = 0$ and $\sigma = 0$, (b) $A = 0.7$ and $\sigma = 0$, (c) $A = 0.7$ and $\sigma = 0.1$, and (c) $A = 0.7$ and $\sigma = 0.5$.

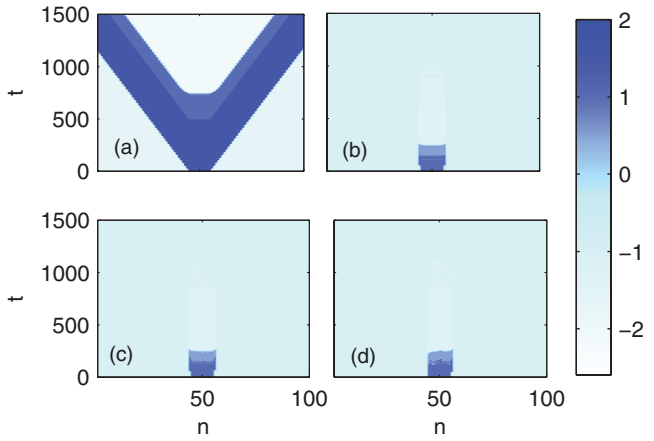

FIG. 6. (Color online) Same graphs as in Fig. 5 but the coupling strength is larger $D = 0.02$ and the variable parameters are (a) $A = 0$ and $\sigma = 0$, (b) $A = 1.1$ and $\sigma = 0$, (c) $A = 1.1$ and $\sigma = 0.1$, and (c) $A = 1.1$ and $\sigma = 0.5$.

Notice that the effect of an enhanced propagation of a harmonic low-frequency signal under the action of a HFS has been observed in numerical simulations of the model of Barkley *et al.* [31] in Ref. [11], but no theoretical treatment of the results has been presented. Moreover, the crucial role of the discreetness of the excitable system for the existence of this effect has not been highlighted.

In Fig. 6 we demonstrate the effect of suppression of pulse propagation. Here all the parameters are the same as in Fig. 5 except for the coupling strength, which is now increased to the value $D = 0.02$, so that the system without HFS admits pulse propagation. The two propagating pulses in the free system ($A = 0$) are shown in Fig. 6(a). Figure 6(b) demonstrates the propagation failure in the presence of a HFS with the parameter $A = 1.1$. Figures 6(c) and 6(d) show the same effect when the noise is superimposed upon the system. We see that even large noise does not destroy the effect of propagation failure. This suggests that the effect of the suppression of pulse propagation is less sensitive to the noise than the effect of the enhancement of propagation.

VI. CONCLUSION

We have analyzed the effect of a homogeneous high-frequency stimulation on the simple model of a myelinated axon described by spatially discrete FitzHugh-Nagumo equations. We have shown that, depending on the amplitude, the HFS may either suppress or enhance the pulse propagation through the axon. This differs essentially from the case of unmyelinated axons described by spatially continuous FHN equations, where the high-frequency stimulation can cause only suppression [10].

Our analysis is based on two main approximations. The first utilizes different time scales of the neuron and the high-frequency signal. Applying the method of averaging, we eliminate the high-frequency term and reduce the problem to the analysis of autonomous systems that describe the slow motion. It appears that the HFS influences the slow dynamics through a parameter A equal to the ratio of the amplitude to the frequency of the HFS. The second approximation is related to the solution of the averaged equations. Here we utilize the smallness of the parameter ε, which defines the ratio between the time scales of the membrane potential and the recovery variable. We adapt the asymptotic methods developed for the free FHN system and derive the main characteristics of the traveling pulse versus the stimulation parameter A.

As an important result of this approach, we have established an analytical criterion for propagation failure and revealed the mechanism underling the effects of enhancement and suppression of pulse propagation. We have shown that the effects are related to the fact that the HFS with a small parameter A reduces the excitability threshold of excitable elements, while the HFS with large A increases the threshold.

The validity of the above two approximations is supported by numerical simulations of the averaged equations and the original system. We have also performed numerical simulations of the original system with the superimposed noise and shown that the effect of suppression of pulse propagation is less sensitive to the noise than the effect of enhancement of propagation.

To summarize, we have shown that the HFS is an efficient tool to control pulse propagation in spatially discrete systems consisting of coupled excitable elements and revealed the mechanism of this control. Our results may be relevant for different fields, including communication technologies, chemistry, neuroscience, and medicine. Specifically, the ability of HFS to suppress and enhance pulse propagation in myelinated axons may partially explain the dual nature (inhibition and activation) of the effect of high-frequency deep-brain stimulation widely discussed in the literature [16–18].

ACKNOWLEDGMENT

This research was funded by the European Social Fund under the Global Grant measure (Grant No. VP1-3.1-ŠMM-07-K-01-025).

APPENDIX: DERIVATION OF AVERAGED EQUATIONS FOR THE DISCRETE FHN MODEL UNDER HFS

Our aim is to simplify the nonautonomous system (1) for large frequencies $\omega \gg 1$, when the period of HF oscillations is much less than the characteristic time scales of the FHN axon. Using the small parameter $\omega^{-1} \ll 1$, we seek to eliminate the HF term $a\cos(\omega t)$ and obtain an autonomous system, the solutions of which approximate the original system. First, we change the variables of the system (1) by using the substitution

$$v_n = V_n + A\sin(\omega t), \tag{A1a}$$

$$w_n = W_n, \tag{A1b}$$

with

$$A = a/\omega, \tag{A2}$$

and derive the following equations for the new variables V_n and W_n:

$$\dot{V}_n = f[V_n + A\sin(\omega t)] - W_n + D(V_{n+1} - 2V_n + V_{n-1}), \tag{A3a}$$

$$\dot{W}_n = \varepsilon[V_n + A\sin(\omega t) + \beta - \gamma W_n]. \tag{A3b}$$

For $A = 0$ and $a = 0$, the systems (A3) and (1) coincide and have identical solutions. Let us denote these solutions by $V_n^0(t) = v_n^0(t)$ and $W_n^0(t) = w_n^0(t)$, where by a zero superscript we mean that the corresponding parameters A or a are zeros. Our aim is to obtain an approximate solution of the system (A3) for $A \neq 0$. If we fix the amplitude a of HFS and increase the frequency ω, the parameter A varies as $O(\omega^{-1})$. In this case an approximate solution of the system (A3) can be obtained by the regular perturbation theory and presented in the form $V_n(t) = v_n^0(t) + O(\omega^{-1})$ and $W_n(t) = w_n^0(t) + O(\omega^{-1})$. Due to the relation (A1) an approximate solution of the original system (1) has the same form: $v_n(t) = v_n^0(t) + O(\omega^{-1})$ and $w_n(t) = w_n^0(t) + O(\omega^{-1})$. We see that for any fixed a and $\omega \to \infty$ the effect of HFS on the system vanishes since $v_n(t) \to v_n^0(t)$ and $w_n(t) \to w_n^0(t)$.

In order to get an appreciable effect from the HFS for large ω, the parameter A must not vanish for $\omega \to \infty$. This can be achieved if with the increase of ω the amplitude a will be increased proportionally as well, $a \propto \omega$. In other words, we have to assume $A = O(1)$ and $a = O(\omega)$. These assumptions lead to a nontrivial perturbation theory. By rescaling the time variable $t = \omega\tau$ (here τ is the "fast" time) the system (A3) can be transformed to the standard form of equations discussed in the method of averaging [28]:

$$\frac{dV_n}{d\tau} = \omega^{-1}\{f[V_n + A\sin(\tau)] - W_n + D(V_{n+1} - 2V_n + V_{n-1})\}, \tag{A4a}$$

$$\frac{dW_n}{d\tau} = \omega^{-1}\varepsilon[V_n + A\sin(\tau) + \beta - \gamma W_n]. \tag{A4b}$$

Due to the small parameter $\omega^{-1} \ll 1$ the variables V_n and W_n vary slowly while the periodic functions on the rhs oscillate fast. According to the method of averaging [28], an approximate solution of the system (A4) can be obtained by averaging the rhs of the system over fast oscillations. Specifically, let us denote the variables of the averaged system by $(\bar{v}_n, \bar{w}_n)$. They satisfy the equations

$$\frac{d\bar{v}_n}{d\tau} = \frac{1}{2\pi\omega}\int_0^{2\pi}\{f[\bar{v}_n + A\sin(\vartheta)] - \bar{w}_n + D(\bar{v}_{n+1} - 2\bar{v}_n + \bar{v}_{n-1})\}d\vartheta, \tag{A5a}$$

$$\frac{d\bar{w}_n}{d\tau} = \frac{\varepsilon}{2\pi\omega}\int_0^{2\pi}[\bar{v}_n + A\sin(\vartheta) + \beta - \gamma\bar{w}_n]d\vartheta. \tag{A5b}$$

The method of averaging states that the averaged system (A5) approximates the solutions of the system (A4) with accuracy

$O(\omega^{-1})$, i.e., $V_n = \bar{v}_n + O(\omega^{-1})$ and $W_n = \bar{w}_n + O(\omega^{-1})$. After calculating the integrals and returning to the original time scale (the overdot denotes differentiation with respect to the original time t), the averaged system (A5) simplifies to

$$\dot{\bar{v}}_n = \bar{f}(\bar{v}_n) - \bar{w}_n + D(\bar{v}_{n+1} - 2\bar{v}_n + \bar{v}_{n-1}), \quad \text{(A6a)}$$

$$\dot{\bar{w}}_n = \varepsilon(\bar{v}_n + \beta - \gamma\bar{w}_n), \quad \text{(A6b)}$$

where $\bar{f}(\bar{v}_n) = (1 - A^2/2)\bar{v}_n - \bar{v}_n^3/3$. Finally, the solution of the original nonautonomous system (1) can be presented as a sum of the solution of the averaged (autonomous) system (A6) that describes the slow motion and the high-frequency term:

$$v_n = \bar{v}_n + A\sin(\omega t) + O(\omega^{-1}), \quad \text{(A7a)}$$

$$w_n = \bar{w}_n + O(\omega^{-1}). \quad \text{(A7b)}$$

We stress that averaged equations (A6) depend only on the parameter A, which is equal to the ratio of the amplitude to the frequency of the HFS. Thus this ratio completely defines the effect of the HFS on the averaged system's dynamics. For example, the effect of HFS is the same if we fix the amplitude a and double the frequency ω or fix the frequency ω and halve the amplitude a. Note that the approximation (A7) is valid for any fixed A including the small values of this parameter; however, as noted above, the effect of HFS vanishes for $A \to 0$.

[1] R. M. Mantel and D. Barkley, Phys. Rev. E **54**, 4791 (1996).
[2] H. G. Othmer and M. Xie, J. Math. Biol. **39**, 139 (1999).
[3] Y. Yu, W. Wang, J. Wang, and F. Liu, Phys. Rev. E **63**, 021907 (2001).
[4] P. Parmananda, H. Mahara, T. Amemiya, and T. Yamaguchi, Phys. Rev. Lett. **87**, 238302 (2001).
[5] T. Yanagita, Y. Nishiura, and R. Kobayashi, Phys. Rev. E **71**, 036226 (2005).
[6] S. Zambrano, J. M. Seoane, I. P. Mariño, M. A. F. Sanjuán, S. Euzzor, R. Meucci, and F. T. Arecchi, New J. Phys. **10**, 073030 (2008).
[7] K. Kilgore and N. Bhadra, Med. Biol. Eng. Comput. **42**, 394 (2004).
[8] C. Tai, W. C. de Groat, and J. R. Roppolo, IEEE Trans. Neural Syst. Rehabil. Eng. **13**, 415 (2005).
[9] D. Cubero, J. P. Baltanás, and J. Casado-Pascual, Phys. Rev. E **73**, 061102 (2006).
[10] I. Ratas and K. Pyragas, Nonlin. Dyn. **67**, 2899 (2012).
[11] E. Ullner, A. Zaikin, J. Garcia-Ojalvo, R. Báscones, and J. Kurths, Phys. Lett. A **312**, 348 (2003).
[12] H. Yu, J. Wang, C. Liu, B. Deng, and X. Wei, Chaos **21**, 043101 (2011).
[13] N. Bhadra, N. Bhadra, K. Kilgore, and J. K. Gustafson, J. Neural Eng. **3**, 180 (2006).
[14] D. M. Ackermann, Jr., N. Bhadra, E. L. Foldes, and K. L. Kilgore, Med. Biol. Eng. Comput. **49**, 241 (2011).
[15] A. L. Benabid, P. Pollak, C. Gervason, D. Hoffmann, D. M. Gao, M. Hommel, J. E. Perret, and J. de Rougemont, Lancet **337**, 403 (1991).
[16] M. L. Kringelbach, N. Jenkinson, S. L. F. Owen, and T. Z. Aziz, Nat. Rev. Neurosci. **8**, 623 (2007).
[17] C. C. Cameron, C. McIntyrea, M. Savasta, L. K.-L. Goff, and J. L. Vitek, Clin. Neurophys. **115**, 1239 (2004).
[18] E. B. Montgomery, Jr. and J. T. Gale, Neurosci. Biobehav. Rev. **32**, 388 (2008).
[19] R. A. FitzHugh, Biophys. J. **1**, 445 (1961).
[20] J. Nagumo, S. Arimoto, and S. Yoshizawa, Proc. IRE **50**, 2061 (1962).
[21] J. Keener and J. Sneyd, *Mathematical Physiology* (Springer, Berlin, 2001).
[22] J. P. Keener, SIAM J Appl. Math. **47**, 556 (1987).
[23] T. Erneux and G. Nicolis, Physica D **67**, 237 (1993).
[24] V. Booth and T. Erneux, SIAM J. Appl. Math. **55**, 1372 (1995).
[25] A. Carpio and L. L. Bonilla, Phys. Rev. Lett. **86**, 6034 (2001).
[26] A. Carpio and L. L. Bonilla, SIAM J Appl. Math. **63**, 619 (2002).
[27] A. Carpio and L. L. Bonila, SIAM J. Appl. Math **63**, 1056 (2003).
[28] J. A. Sanders, F. Verhulst, and J. Murdock, *Averaging Methods in Nonlinear Dynamical Systems* (Springer, Berlin, 2007).
[29] J. K. Kevorkian and J. D. Cole, *Multiple Scale and Singular Perturbation Methods* (Springer, Berlin, 1996).
[30] J. P. Keener, SIAM J. Appl. Math. **39**, 528 (1980).
[31] D. Barkley, M. Kness, and L. S. Tuckerman, Phys. Rev. A **42**, 2489 (1990).